

Characterizing Hydrogen Bonding in Uracil–Nitrosamine Complexes through One- and Two-Bond Spin–Spin Coupling Constants across Hydrogen Bonds

Hossein Roohi*[1] and Elham Anjomshoa[2]

[1]Department of Chemistry, Faculty of Science, University of Guilan, P. O. Box 41335-1914, Rasht, Iran

[2]Department of Chemistry, Faculty of Science, University of Sistan and Baluchestan, Zahedan, Iran

Received December 13, 2010; E-mail: hroohi@guilan.ac.ir, hrouhi@gmail.com

One- and two-bond spin–spin coupling constants, ^{1}J, ^{1h}J, and ^{2h}J across X–H···Y hydrogen bonds and isotropic chemical shift of bridging hydrogens have been computed for complexes formed from interaction between the parent nitrosamine (**NA**) and four preferential binding sites of the uracil (**U**) at B3LYP/6-311++G(2d,2p)//MP2/6-311++G(2d,2p) level of theory. All complexes are stabilized by two H_U···Y and H_{NA}···Y hydrogen bonds. The correlation between spin–spin coupling constants ($^{1h}J_{H\cdots Y}$ and $^{2h}J_{X\cdots Y}$) and isotropic chemical shifts with the binding energy, H-bond distance, red shift of vibration frequency, charge-transfer energy, and electron density at H-bond critical point were investigated at the above-mentioned level of theory. Change in nucleus-independent chemical shift of **U** ring upon complex formation was also calculated.

Nuclear magnetic resonance (NMR) spectroscopy yields chemical shifts (σ_A) and nuclear spin–spin coupling constants (J_{AB}) for magnetic nuclei A and B, arising from magnetic and spin interactions that are absent in nonrelativistic (Schrödinger) theory but appear naturally in relativistic quantum field theory. NMR spectra are a very valuable source of information on the molecular structure due to the sensitivity of measured parameters to the changes in the conformation of a molecule and to the influence of the environment. Nuclear magnetic resonance (NMR) is in particular a routine tool to analyze H-bonding interactions in various systems[1–7] The NMR criteria are more valuable than the structural ones, since they are applicable not only to crystals but to neat liquids and solutions as well. Conventionally, magnetic shielding constants (or chemical shifts) and especially spin–spin coupling constants ^{1}J have been used for this purpose.[8] The nuclear spin–spin coupling constants are unique evidence for hydrogen-bond formation. Thus, application of nuclear spin–spin coupling constants for the analysis of hydrogen-bonded complexes has become an emerging area of research.[9–18]

In the present paper, we have investigated intermolecular dihydrogen bonds formed from interaction between **NA** and **U**. All complexes stabilized by intermolecular H-bonds have been characterized in terms of their structures, binding energies, isotropic chemical shift, and spin–spin coupling constants. The correlations between the NMR spectroscopic properties and binding energy, H-bond distance, electron density topography, and charge-transfer energy have been investigated. We have also examined change in aromaticity of **U** ring upon complex formation.

Computational Details

The geometry optimizations were performed using MP2, B3LYP, and B3PW91 methods in conjunction with 6-311++G(2d,2p) basis set. Vibrational frequencies calculated using the B3LYP and B3PW91 methods were used to characterize stationary points as minima (number of imaginary frequency (NIF) = 0) or transition state (NIF = 1) and to evaluate zero-point vibrational energies (ZPVE). The counterpoise procedure (CP)[19] was used to correct for basis set superposition error (BSSE) in the calculation of binding energies. Spin–spin coupling constants involving ^{13}C, ^{15}N, ^{17}O, and ^{1}H in all monomers and complexes were computed at B3LYP/6-311++G(2d,2p) level on the structures optimized at MP2/6-311++G(2d,2p) level of theory. Because of introduction of exact exchange in the B3LYP exchange–correlation functional, errors for the prediction of spin–spin coupling constants relative to experiment are reduced further: indeed, the performance of hybrid methods is better than that of the CASSCF method. Recalling that DFT is applicable to a much broader range of molecules than CASSCF theory, this observation illustrates the usefulness of DFT for the prediction of spin–spin coupling constants.[20]

In the Ramsey approximation,[21,22] the total coupling constant (J) is a sum of four contributions: the paramagnetic spin–orbit (PSO), diamagnetic spin–orbit (DSO), Fermi-contact (FC), and spin–dipole (SD). In the calculations presented here, all four terms that contribute to nuclear spin–spin coupling constants in nonrelativistic theory have been calculated. The PSO and DSO terms account, respectively, for the interaction between the nuclear spins and the orbital angular momentum of the electrons, whereas the FC and SD terms account, respectively, for the interaction between the nuclear and electronic spins and the presence of the electronic spins in the nuclear positions.

The NMR spin Hamiltonian is usually expressed not in terms of the reduced indirect spin–spin coupling tensors, $\mathbf{K}_{KL}$,

Published on the web July 2, 2011; doi:10.1246/bcsj.20100350

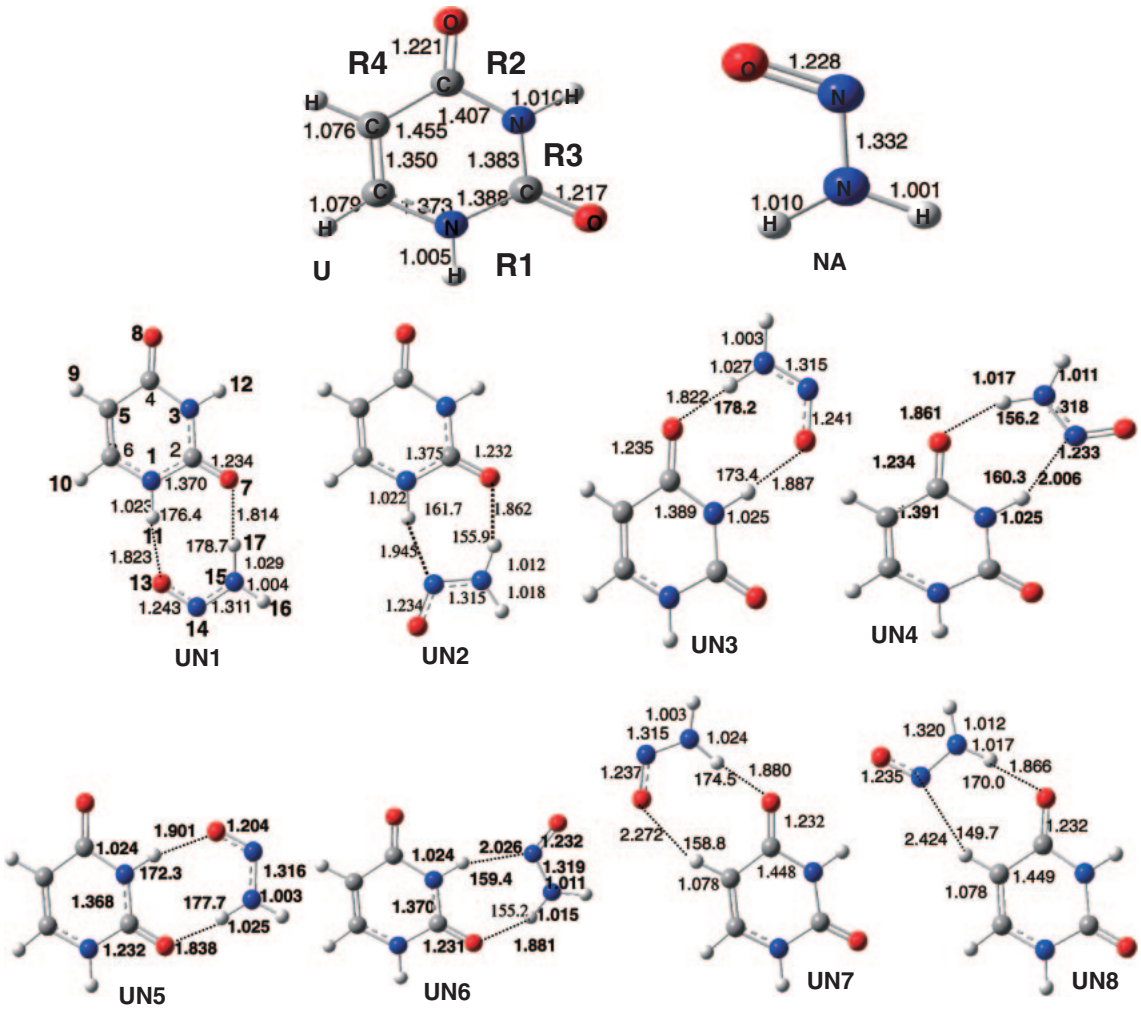

Figure 1. The optimized structures and selected geometrical parameters (Å and °) for free monomers and complexes **U**–**NA** at MP2/6-311++G(2d,2p) level.

but rather in terms of the indirect spin–spin coupling tensors $\mathbf{J}_{KL}$, which are related to the reduced tensors as:[23]

$$\mathbf{J}_{KL} = h\frac{\gamma_K}{2\pi}\frac{\gamma_L}{2\pi}\mathbf{K}_{KL} \quad (1)$$

where γ_K and γ_L are the magnetogyric ratios of nuclei K and L. Thus, the sign of J is a function of the magnetogyric ratio of the nuclei involved in interaction. The magnetogyric ratios of ^{1}H and ^{13}C are positive and those of ^{15}N and ^{17}O are negative.

Schleyer et al.[24–26] have proposed a simple and efficient probe for aromaticity: Nucleus-independent chemical shift (NICS), which is computed as the negative magnetic shielding at some selected point in space, e.g., at a ring or cage center. Negative NICS values denote aromaticity and positive NICS values denote antiaromaticity while small NICS values indicate nonaromaticity. We have calculated NICS values for all MP2 optimized structures at the B3LYP/6-311++G(2d,2p)//MP2/6-311++G(2d,2p) level with the gauge-including atomic orbital (GIAO) formalism.[27,28]

Topological properties were calculated at MP2/6-311++G(2d,2p) level of theory using AIM2000 program package.[29] The NBO analysis was carried out at the HF/6-311++G(2d,2p)//MP2/6-311++G(2d,2p) level of theory using version 3.1 of NBO package[30] included in Gaussian 03 program package.[31]

Results and Discussion

The optimized structures obtained from interaction between uracil (**U**) and **NA** are depicted in Figure 1. As can be seen in Figure 1, in **U**–**NA** complexes, **NA** can be placed in four regions R1 to R4 in vicinity of **U**. For each region, two stable structures are found on the potential surface. Both structures are cyclic with two hydrogen bonds involved in the interaction. Thus, eight optimized structures were found on the potential surface of interaction. In eight-membered cyclic complexes **UN1**, **UN3**, **UN5**, and **UN7**, the O atom of **NA** and one C=O group of **U** act as proton acceptors and N–H bond of **NA** and **U** (with the exception of C–H bond in **UN8**) as proton donors. In seven-membered cyclic structures **UN2**, **UN4**, **UN6**, and **UN8**, instead of O atom, the N atom of NO group in **NA** acts as a proton acceptor. Thus, two H-bond interactions $H_U\cdots O(N)_{NA}$ and $H_{NA}\cdots O_U$ can be seen in all complexes. The binding energies calculated at various levels of theory are listed in Table 1. The charge-transfer energy, electron density at H-bond critical point, and electron density on the bridged H atom are collected in Table 2.

One-Bond Spin–Spin Coupling Constants. The intermolecular spin–spin coupling constants (SSCCs) ^{1}J(X–H) and ^{1h}J(H–Y) and the their components (PSO, DSO, FC, and SD) across the X–H···Y hydrogen bonds (N(C)–H_U···$O(N)_{NA}$ and N–H_{NA}···O_U) in **U**–**NA** complexes are given in Table 3. As can be seen in this table, the main contribution to J is the FC term followed by the PSO term. The absolute values of FC terms are smaller than those of ^{1}J(X–H) ones. The most interesting feature of these coupling constants is that all one-bond coupling constants ^{1}J(X–H) are negative and those of ^{1h}J(H···Y) are positive. Since the magnetogyric ratio of ^{1}H is positive and those of ^{15}N and ^{17}O are negative, all reduced H···N(O) coupling constants $^{1h}K_{H\cdots N(O)}$ across X–H···Y hydrogen bonds are negative. We have also calculated spin–spin coupling constants using cc-pVDZ basis set. The selected values for **UN1** and **UN2** are given as supplementary data in Tables S1 and S2. As can be seen, FC values are sensitive to the quality of basis function, but the FC term in all cases is dominant remarkably.

Table 1. Calculated Binding Energies (kJ mol^{-1}) of the **UN1–8** Complexes Using B3LYP, B3PW91, and MP2 Methods in Combination with 6-311++G(2d,2p) Basis Set

	ΔE_1[a)]	ΔE_2[b)]	ΔE_3[c)]	ΔE_1[a)]	ΔE_2[b)]	ΔE_3[c)]
	UN1			**UN2**		
B3LYP	−39.5	−38.0	−30.4	−33.7	−32.2	−25.1
B3PW91	−53.1	−51.1	−43.3	−47.6	−45.9	−38.5
MP2	−63.2	−53.3	−45.6	−60.9	−51.6	−44.4
	UN3			**UN4**		
B3LYP	−28.1	−26.6	−19.9	−25.0	−23.5	−17.1
B3PW91	−41.4	−40.1	−33.2	−38.6	−37.5	−30.9
MP2	−52.2	−42.7	−35.9	−51.2	−42.3	−35.8
	UN5			**UN6**		
B3LYP	−24.0	−22.5	−16.1	−21.2	−19.7	−13.5
B3PW91	−36.9	−35.1	−28.5	−34.5	−32.9	−26.6
MP2	−49.2	−39.9	−33.5	−48.3	−39.6	−33.5
	UN7			**UN8**		
B3LYP	−19.7	−18.2	−12.1	−20.0	−18.5	−12.7
B3PW91	−32.4	−31.5	−25.2	−33.0	−32.4	−26.3
MP2	−42.5	−35.4	−29.4	−44.0	−37.2	−31.3

a) ΔE_1: Electronic binding energy. b) $\Delta E_2 = \Delta E_1 + \text{BSSE}$. c) $\Delta E_3 = \Delta E_2 + \Delta\text{ZPVE}$.

The observed changes of ^{1}J in all complexes are dominated mainly by changes in two largest contributions, FC and PSO terms. The change in $^{1}J(\text{N–H})_U$ is small by complex formation. It is difficult to recognize any regular pattern in changes of ^{1}J of $(\text{N–H})_U$ involved in interaction upon complexation. The absolute value of ^{1}J of $(\text{N–H})_{NA}$ involved in interaction increases upon complex formation by ≈3.0 Hz. Increase of the O–H distance leads to decrease in the absolute value of the coupling constant, whereas the influence of electronic density of proton acceptor (O_U) increases it, so that the latter effect is dominant.

The SSCC across the hydrogen bond, ^{1h}J(H···Y), are the most remarkable in **U**–**NA** complexes since these intermolecular couplings are direct evidences of the existence of hydrogen bonding between **U** and **NA**. The positive values of the ^{1h}J(H···Y) are also determined by the most dominant FC term followed by the PSO term. The FC terms for H···Y contacts are greater than ^{1h}J ones. Since the sum of negative values of SD and DSO terms is greater than the PSO term, FC terms for these intermolecular interactions are greater than ^{1h}J ones.

The magnitude of $^{1h}J(H_U\cdots Y)$ coupling constants ranges from 5.43 Hz for **UN1** to 0.84 Hz for **UN7** and 2.85 Hz for **UN2** to 0.87 Hz for **UN8**. The value of $^{1h}J(H_{NA}\cdots Y)$ changes from 6.12 Hz in **UN1** to 5.42 Hz in **UN7** and 5.13 Hz in **UN2** to 4.97 Hz in **UN8**. As can be seen, intermolecular coupling constants decrease in going from **UN1** to **UN7** and from **UN2** to **UN8**, indicating the most stable complex has greater intermolecular SSCC. In addition, these SSCCs for eight-membered ring complexes are greater than seven-membered ones in agreement with greater binding energy (BE) of the former with respect to the latter. Thus, magnitude of intermolecular CC ^{1h}J(H···Y) can be considered as a reliable criterion of strength or covalent nature of H-bonding in **U**–**NA** complexes. From comparison of coupling constants, it is predicted that the H_{NA}···Y H-bonds are stronger than H_U···Y ones. There is a relationship between electronic BE and the sum of $^{1h}J(H_{NA}\cdots Y)$ and $^{1h}J(H_U\cdots Y)$ SSCCs in **U**–**NA** complexes. This correlation is depicted in Figure 2. **UN1** with greater BE has greater $^{1h}J(H_{NA}\cdots Y) + {}^{1h}J(H_U\cdots Y)$. The linear correlation between the sum of $^{1h}J(H_{NA}\cdots Y)$ and $^{1h}J(H_U\cdots Y)$ SSCCs and the sum of electron densities at corresponding hydrogen-bond critical points, HBCPs, are depicted in Figure 3 with correlation coefficient of 0.980 and 0.991 for eight- and seven-membered ring complexes, respectively.

Table 2. Charge-Transfer Energy (kcal mol^{-1}), Electron Density at H-Bond Critical Point, and Electron Density on the Bridged H Atom at MP2/6-311++G(2d,2p) Level[a)]

	UN1	**UN2**	**UN3**	**UN4**	**UN5**	**UN6**	**UN7**	**UN8**
$E^{(2)}$[b)] ($\sigma \rightarrow \sigma^*$)								
LP[c)](Y)$_U$ → σ^*(X–H)$_{NA}$	20.82	14.75	19.61	14.37	18.07	12.99	14.99	14.78
LP(Y)$_{NA}$ → σ^*(X–H)$_U$	20.95	15.51	15.91	12.53	14.78	11.59	30.03	2.23
$\rho(H_U\cdots Y_{NA})$/au	0.0314	0.0288	0.0265	0.0248	0.0255	0.0238	0.0125	0.0108
$\rho(H_{NA}\cdots Y_U)$/au	0.0315	0.0286	0.0308	0.0287	0.0294	0.0272	0.0265	0.0279
$\rho(H_U\cdots)$/au	0.4514	0.4773	0.4549	0.4774	0.4568	0.4801	0.8677	0.8956
$\rho(H_{NA}\cdots)$/au	0.4452	0.4506	0.4489	0.4553	0.4528	0.4630	0.4601	0.4627

a) The $H_U\cdots$ and $H_{NA}\cdots$ denote H atom of U and NA involved in H-bonding, respectively. b) Charge-transfer energy. c) Lone pair.

Table 3. One-Bond Spin–Spin Coupling Constants ^{1}J, ^{1h}J, and Their Components (Hz) at B3LYP/6-311++G(2d,2p)//MP2/6-311++G(2d,2p) Level

Compound		FC	SD	PSO	DSO	$^{1}J/^{1h}J$
UN1	N1–H11	−87.63	−0.18	−1.02	−0.55	−89.37
	O13···H11	6.05	−0.75	0.81	−0.68	5.43
	O7···H17	6.14	−0.40	1.04	−0.67	6.12
	N15–H17	−86.35	−0.21	−0.64	−0.42	−87.62
	N15–H16	−89.20	−0.20	−1.52	−0.32	−91.24
	C2–O7	18.98	−0.90	10.21	−0.15	28.15
UN2	N1–H11	−87.28	−0.19	−1.12	−0.53	−89.12
	N14···H11	3.64	−0.49	0.24	−0.54	2.85
	O7···H16	5.15	−0.38	0.98	−0.63	5.13
	C2–O7	18.98	−0.99	10.22	−0.15	28.07
	N15–H17	−81.18	−0.22	−1.51	−0.35	−83.26
	N15–H16	−96.52	−0.23	−0.62	−0.39	−97.76
UN3	N3–H12	−84.33	−0.13	−1.03	−0.57	−86.06
	O13···H12	5.18	−0.68	0.81	−0.68	4.64
	O8···H17	6.11	−0.47	1.05	−0.66	6.04
	C4–O8	18.57	−1.11	12.49	−0.13	29.82
	N15–H17	−86.55	−0.21	−0.65	−0.42	−87.83
	N15–H16	−88.75	−0.21	−1.58	−0.32	−90.87
UN4	N3–H12	−83.68	−0.13	−1.10	−0.56	−85.46
	N14···H12	3.25	−0.44	0.24	−0.53	2.51
	O8···H16	5.19	−0.46	1.01	−0.63	5.11
	C4–O8	18.79	−1.20	12.50	−0.13	29.97
	N15–H17	−80.54	−0.22	−1.55	−0.35	−82.66
	N15–H16	−96.27	−0.22	−0.63	−0.39	−97.51
UN5	N3–H12	−84.34	−0.13	−1.04	−0.56	−86.08
	O13···H12	5.04	−0.65	0.83	−0.67	4.54
	O7···H17	6.00	−0.38	1.00	−0.66	5.96
	C2–O7	18.80	−0.95	10.19	−0.15	27.90
	N15–H17	−86.53	−0.20	−0.69	−0.42	−87.83
	N15–H16	−89.07	−0.22	−1.59	−0.32	−91.20
UN6	N3–H12	−83.82	−0.13	−1.11	−0.55	−85.62
	O7···H16	5.02	−0.37	0.95	−0.63	4.98
	N14···H12	3.20	−0.44	0.23	−0.52	2.47
	C2–O7	18.91	−1.02	10.21	−0.15	27.96
	N15–H17	−80.81	−0.22	−1.55	−0.35	−82.93
	N15–H16	−96.27	−0.22	−0.68	−0.39	−97.56
UN7	C5–H9	169.66	0.23	0.09	1.07	171.05
	O8···H17	5.42	−0.42	1.05	−0.63	5.42
	O13···H9	1.14	−0.38	0.51	−0.43	0.84
	C4–O8	17.95	−1.26	12.61	−0.13	29.17
	N15–H17	−86.60	−0.19	−0.73	−0.40	−87.93
	N15–H16	−88.66	−0.22	−1.63	−0.32	−90.82
UN8	C5–H9	167.80	0.22	0.16	1.06	169.24
	O8···H16	5.03	−0.48	1.04	−0.62	4.97
	N14···H9	1.17	−0.17	0.20	−0.34	0.87
	C4–O8	18.11	−1.27	12.63	−0.13	29.34
	N15–H17	−79.08	−0.21	−1.59	−0.35	−81.24
	N15–H16	−95.60	−0.21	−0.66	−0.38	−96.85
U	N1–H11	−87.18	−0.25	−1.97	−0.45	−89.85
	N3–H12	−83.15	−0.16	−1.77	−0.48	−85.56
	C5–H9	162.26	0.19	0.45	0.95	163.85
	C2–O7	20.91	−1.66	10.42	−0.13	29.54
	C4–O8	19.95	−1.92	12.84	−0.11	30.76
	N15–H17	−82.58	−0.21	−1.47	−0.31	−84.57
NA	N15–H16	−92.82	−0.23	−1.52	−0.28	−94.85

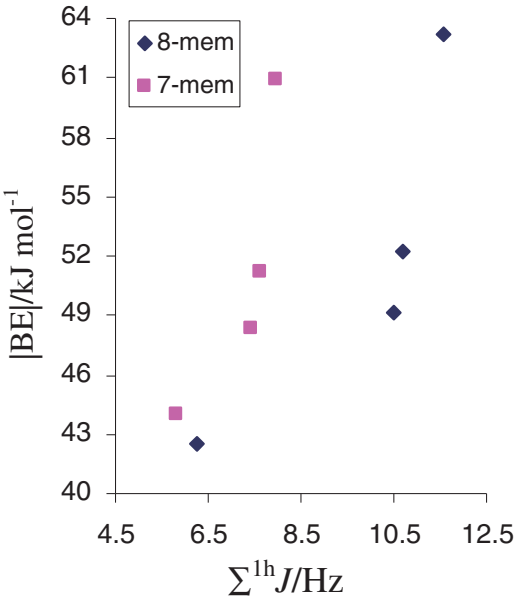

Figure 2. Correlation between absolute BE and sum of $^{1h}J(H_{NA}\cdots Y)$ and $^{1h}J(H_{U}\cdots Y)$ SSCCs in eight- and seven-membered ring complexes.

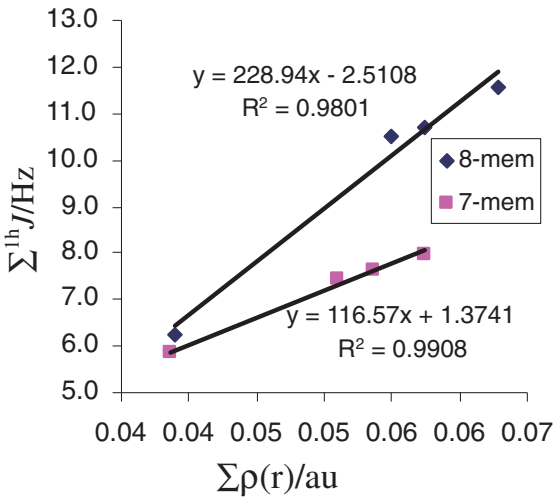

Figure 3. Correlation between the sum of $^{1h}J(H_{NA}\cdots Y)$ and $^{1h}J(H_{U}\cdots Y)$ SSCCs and the sum of $\rho(r)$ at the corresponding HBCPs in eight- and seven-membered ring complexes.

Two-Bond Spin–Spin Coupling Constants. Total $^{2h}J_{N(C)\cdots O(N)}$ and $^{2h}J_{O\cdots N}$ two-bond coupling constants across the $N–H_U\cdots O(N)_{NA}$ and $N–H_{NA}\cdots O_U$ hydrogen bonds and their components (PSO, DSO, FC, and SD) for the complexes **UN1–8** are reported in Table 4. The sign of $^{2h}J_{X\cdots Y}$ is negative if the magnetogyric ratio of either X or Y is negative. Because the magnetogyric ratios of ^{1}H and ^{13}C are positive and those of ^{15}N and ^{17}O are negative, all $^{2h}J_{N\cdots O(N)}$ values are positive and those of $^{2h}J_{C\cdots O(N)}$ are negative. The magnitude of $^{2h}J_{N(C)\cdots O(N)}$ ranges from −3.879 Hz in **UN7** to 5.015 in **UN1** and −5.088 Hz in **UN8** to 7.231 in **UN2**. Furthermore, the $^{2h}J_{O\cdots N}$ values are in the range of 3.979 Hz in **UN7** to 4.995 in **UN1** and 5.025 Hz in **UN8** to 5.280 in **UN2**. The main contribution to $^{2h}J_{N(C)\cdots O(N)}$ and $^{2h}J_{O\cdots N}$ is also the FC term. The same trend can

Table 4. Two-Bond Spin–Spin Coupling Constant ^{2h}J and Its Components (Hz) at B3LYP/6-311++G(2d,2p)//MP2/6-311++G(2d,2p) Level

Complex	FC	DSO	PSO	SD	^{2h}J
			$N(C)_U\cdots O(N)$		
UN1	4.934	0.023	−0.073	0.131	5.015
UN3	3.364	0.024	−0.083	0.113	3.418
UN5	3.106	0.023	−0.073	0.107	3.164
UN7	−3.788	−0.044	0.052	−0.098	−3.879
UN2	7.114	0.020	0.041	0.056	7.231
UN4	5.315	0.020	0.032	0.051	5.418
UN6	4.972	0.020	0.033	0.052	5.077
UN8	−5.057	−0.038	0.024	−0.016	−5.088
			$O_U\cdots N$		
UN1	4.985	0.018	−0.110	0.102	4.995
UN3	4.758	0.018	−0.095	0.107	4.788
UN5	4.475	0.018	−0.100	0.092	4.486
UN7	3.939	0.018	−0.068	0.090	3.979
UN2	5.279	0.017	−0.078	0.062	5.280
UN4	5.201	0.017	−0.053	0.074	5.238
UN6	4.942	0.017	−0.084	0.056	4.931
UN8	5.026	0.017	−0.102	0.085	5.025

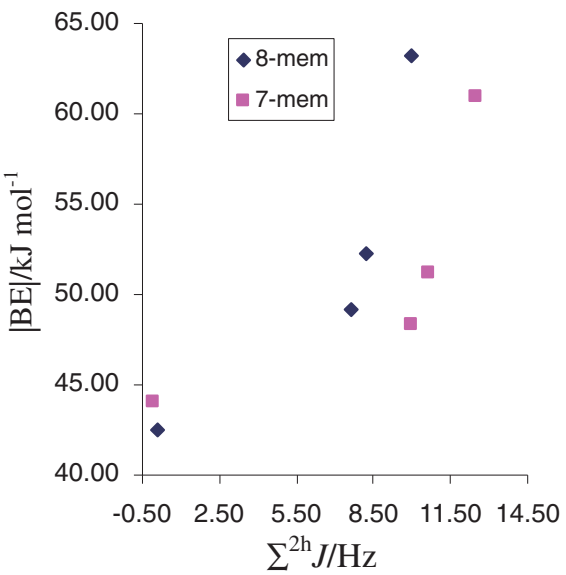

Figure 4. Correlation between absolute BE and the sum of $^{2h}J_{O\cdots N}$ and $^{2h}J_{N(C)\cdots N(O)}$ SSCCs in eight- and seven-membered ring complexes.

be observed for FC terms which are smaller than ^{2h}J ones. The comparison between SSCCs across the $NH\cdots O(N)_{NA}$ and $NH\cdots O_U$ hydrogen bonds shows that the ^{2h}J values are greater than ^{1h}J ones.

The MP2/6-311++G(2d,2p) binding energies (BEs) of complexes in each series correlate with the sum of $^{2h}J_{O\cdots N}$ and $^{2h}J_{N(C)\cdots N(O)}$ SSCCs. This relationship is displayed in Figure 4. It is obvious that the increase in BE is accompanied by increase in ^{2h}J SSCC, although that this correlation is not linear due to the presence of C···O contact in **UN7** and **UN8**.

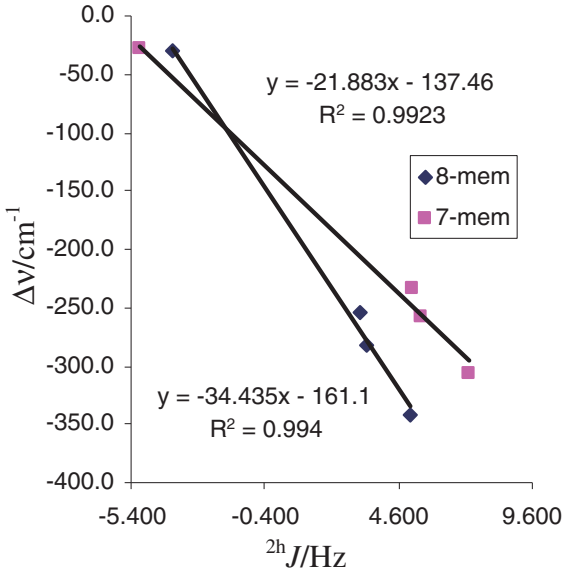

Figure 5. Red shift of $N–H_U$ stretching frequency ($\Delta\nu/cm^{-1}$) versus the $^{2h}J_{N(C)\cdots N(O)}$ SSCC.

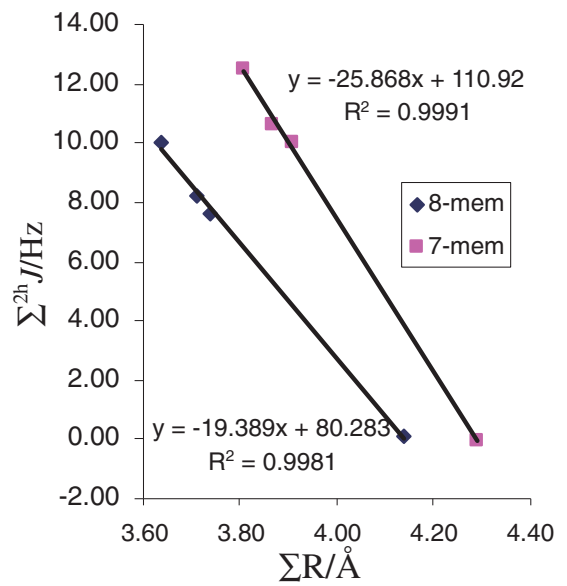

Figure 6. Correlation between the sum of $^{2h}J_{O\cdots N}$ and $^{2h}J_{N(C)\cdots N(O)}$ SSCCs and the sum of corresponding H-bond distances (R) in eight- and seven-membered ring complexes.

Although eight-membered ring complexes are more stable than seven-membered ones, ^{2h}J SSCCs for the former is smaller than the latter.

The red shifts of N(C)–H stretching frequencies ($\Delta\nu$) calculated at B3LYP/6-311++G(2d,2p) level are well correlated with the $^{2h}J_{N(C)\cdots N(O)}$ SSCCs upon H-bond formation in **U–NA** complexes. Figure 5 shows these relationships with correlation coefficients of 0.994 and 0.992 for eight- and seven-membered ring complexes, respectively.

The correlation between the sum of $^{2h}J_{O\cdots N}$ and $^{2h}J_{N(C)\cdots N(O)}$ SSCCs and corresponding H-bond distances are presented in Figure 6. The curves describing these changes have

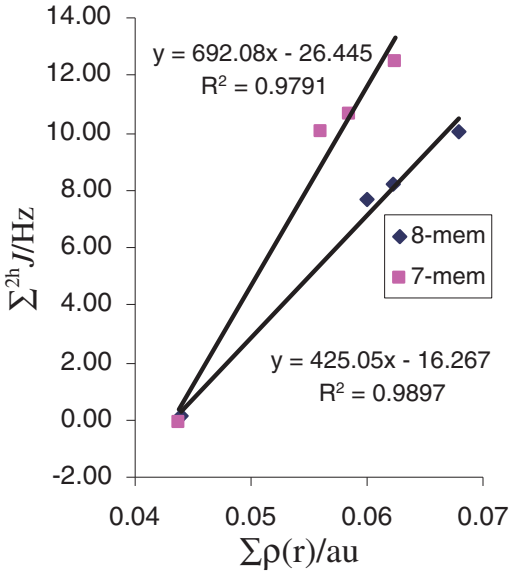

Figure 7. Correlation between the sum of $^{2h}J_{O\cdots N}$ and $^{2h}J_{N(C)\cdots N(O)}$ SSCCs and the sum of $\rho(r)$ at the corresponding HBCPs in eight- and seven-membered ring complexes.

correlation coefficients of 0.998 and 0.999 for eight- and seven-membered ring complexes, respectively. As can be seen, increase in SSCCs in both types of complexes is connected with decrease in H-bond distances. These curves show linear connection between H-bond distance and ^{2h}J in each series, irrespective of whether **U** acts as proton donor or proton acceptor.

Similar to the linear correlation between the H-bond distances and corresponding SSCCs ($^{2h}J_{N(C)\cdots N(O)}$ and $^{2h}J_{O\cdots N}$), ^{2h}J values correlate well with the electron densities $\rho(r)$ at the hydrogen bond critical points (HBCP). The relationship between the sum of $^{2h}J_{N(C)\cdots N(O)}$ and $^{2h}J_{O\cdots N}$ SSCCs and the sum of electron density at $H_U\cdots N(O)_{NA}$ and $H_{NA}\cdots O_U$ HBCPs are depicted in Figure 7. From Table 4 and Figure 7, it is found that the $\rho(r)$ at both types HBCPs has a linear relationship with the ^{2h}J values of eight-membered ring complexes as well as seven-membered ones. As expected for conventional H-bonding contacts, SSCC values in both types of complexes increase as the $\rho(r)$ values at HBCPs increase.

There is a relationship between $^{2h}J_{N(C)\cdots O(N)}$ SSCC and electron density ρ on hydrogen atom involved in N(C)–$H\cdots O(N)_{NA}$ and N–$H\cdots O_U$ interactions (Figures 8 and 9). It is found that increase in ρ is correlated by increase in ^{2h}J.

Correlation between the sum of $^{2h}J_{O\cdots N}$ and $^{2h}J_{N(C)\cdots N(O)}$ SSCCs and the sum of charge-transfer energies $E^{(2)}$ correspond to $LP(N(O))_{NA} \rightarrow \sigma^*(N(C)–H)$ and $LP(O)_U \rightarrow \sigma^*(N–H)$ interactions in eight- and seven-membered ring complexes are shown in Figure 10. Increase in the sum of SSCCs is accompanied with increase in the sum of $E^{(2)}$.

Isotropic Chemical Shifts. The electron density analysis (Table 2) shows that the bridging hydrogen in H-bond interaction loses its electron density, that is, becomes more positively charged. Therefore, as expected in conventional H-bonding systems, protons experiencing hydrogen bond undergo deshielding, which in turn causes a downfield chemical shift. This is another powerful indicator of hydrogen bonding.

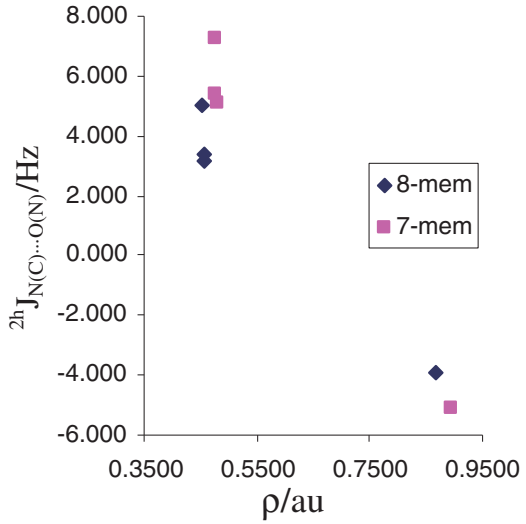

Figure 8. SSCC, $^{2h}J_{N(C)\cdots O(N)}$, as a function of electron density, ρ, on bridged hydrogen atom involved in N(C)–$H\cdots O(N)_{NA}$ interaction.

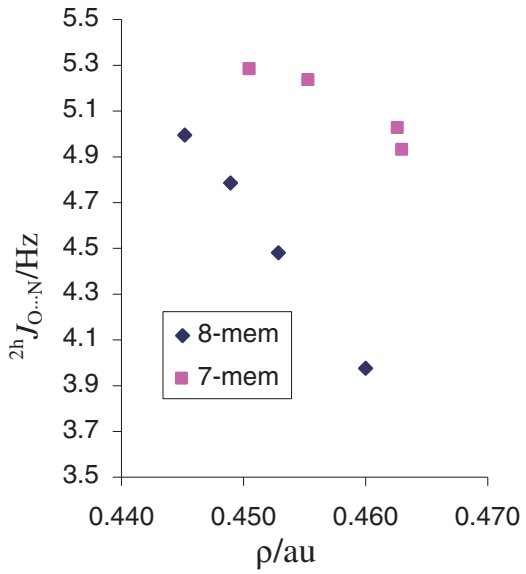

Figure 9. SSCC, $^{2h}J_{O\cdots N}$, as a function of electron density, ρ, on bridged hydrogen atom involved in N–$H\cdots O_U$ interaction.

The changes of isotropic chemical shifts of the bridging hydrogens, $\Delta\sigma_{iso}(H)$, and change of electronic density ($\Delta\rho$) at nuclear critical point are reported in Table 5. As can be seen, changes in isotropic chemical shift of bridging hydrogens $\Delta\sigma_{iso}(H) = \sigma_{iso}^{D–H\cdots A}(H) - \sigma_{iso}^{D–H}(H)$ for all complexes are negative. The negative character of $\Delta\sigma_{iso}(H)$ is explained by the deshielding of the bridging hydrogen H that is induced by the formation of the hydrogen bond. BEs as a function of sum of changes in isotropic chemical shifts $\Delta\sigma_{iso}(H_U\cdots$ and $H_{NA}\cdots)$, ($H_U\cdots$ and $H_{NA}\cdots$ denote H atom of **U** and **NA** involved in H-bonding, respectively), is shown in Figure 11. A good correlation exists between the $\Delta\sigma_{iso}$ and the BE. As can be seen, increase in BE is accompanied with increase in $\Delta\sigma_{iso}$ and in turn increase in deshielding of the bridging hydrogen atoms. The

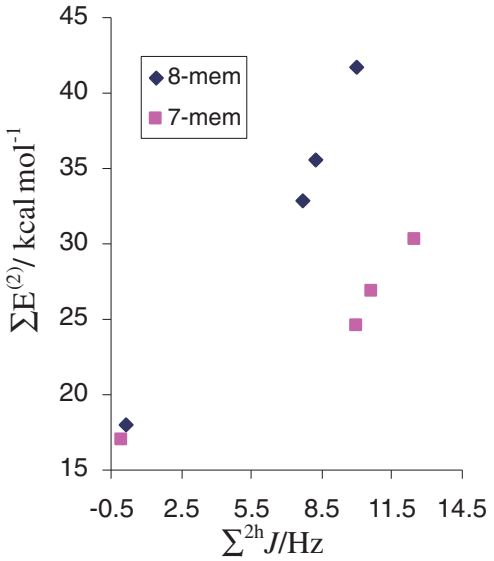

Figure 10. Correlation between the sum of $^{2h}J_{O\cdots N}$ and $^{2h}J_{N(C)\cdots N(O)}$ SSCCs and the sum of charge-transfer energies $E^{(2)}$ correspond to $LP(N(O))_{NA} \rightarrow \sigma^*(N(C)–H)$ and $LP(O)_U \rightarrow \sigma^*(N–H)$ interactions in eight- and seven-membered ring complexes.

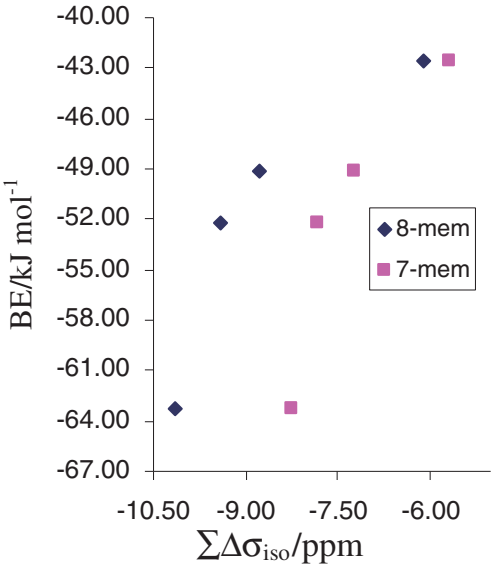

Figure 11. Electronic binding energy, BE, as a function of the sum of change in isotropic chemical shift $\Delta\sigma_{iso}$ of H atoms involved in H-bonding.

Table 5. Changes in NMR Chemical Shifts and Electron Density of Bridging H Caused by Complexation **U** with **NA** at B3LYP/6-311++G(2d,2p)//MP2/6-311++G(2d,2p) Level

Hydrogen	$\Delta\sigma_{iso}$(H)/ppm				$\Delta\rho$/au			
	UN1	**UN2**	**UN3**	**UN4**	**UN1**	**UN2**	**UN3**	**UN4**
$H_U\cdots$	−5.5115	−3.9726	−4.8218	−3.5213	−0.0911	−0.0652	−0.0810	−0.0585
$H_{NA}\cdots$	−4.6257	−4.2847	−4.5856	−4.3007	−0.1106	−0.1060	−0.1069	−0.1013
H_{NA}	−0.1312	−0.3734	−0.0877	−0.3038				
H_U	−0.8052	−0.9456	0.6277	0.6212				
	UN5	**UN6**	**UN7**	**UN8**	**UN5**	**UN6**	**UN7**	**UN8**
$H_U\cdots$	−4.5536	−3.3205	−2.2457	−1.4829	−0.0790	−0.0558	−0.0723	−0.0444
$H_{NA}\cdots$	−4.2161	−3.9071	−3.8629	−4.1784	−0.1030	−0.0936	−0.0957	−0.0939
H_{NA}	−0.0595	−0.2751	−0.1085	−0.3079				
H_U	0.8460	0.7070	−0.2052	−0.1315				

value of $\Delta\sigma_{iso}$ in the most stable complex is greater than others. Figure 12 shows the dependence of $\Delta\sigma_{iso}$ on ($H_U\cdots Y$) and ($H_{NA}\cdots Y$) H-bond distances. As can be seen, the $\Delta\sigma_{iso}$ increases as the HB distance decreases.

The electronic density at $H_U\cdots O(N)$ bond critical point is a criterion for the strength of H-bonding. The loss of electron density on hydrogen atoms has been used as one of the criteria for H-bonding. Figure 13 depicts the relationship between $\Delta\sigma_{iso}(H_U\cdots$ and $H_{NA}\cdots)$ and electronic density, ρ, at $H_U\cdots O(N)$ and $H_{NA}\cdots O$ bond critical points. It is clear that the largest $\Delta\sigma_{iso}$ corresponds to the largest ρ. The relationship between the sum of $\Delta\sigma_{iso}(H\cdots)$ and the sum of change in electronic density $(\Delta\rho)$/au on the H atom involved in H-bonding are shown in Figure 14. The resulting values clearly show that the hydrogen atoms are deshielded upon H-bond formation. It is found that the decrease in electron density of H··· atoms upon H-bonding correlate well with decrease in σ_{iso} and in sequence increase in deshielding of H··· atoms. Accordingly, the calculated NMR properties show a relationship with the electronic characteristics of the hydrogen bond in these complexes.

The correlation between $\Delta\sigma_{iso}(H_U\cdots)$ and charge-transfer energy $E^{(2)}$ corresponding to the $LP(N(O))_{NA} \rightarrow \sigma^*(N(C)–H)$ interactions is illustrated in Figure 15a. This figure shows how the deshielding factor of $H_U\cdots$ depends on the strength of intermolecular interaction. Correlation between sum of $\Delta\sigma_{iso}(H_U\cdots$ and $H_{NA}\cdots)$ and the sum of corresponding charge transfer energies $E^{(2)}$ related to the $LP(N(O))_{NA} \rightarrow \sigma^*(N(C)–H)$ and $LP(O)_U \rightarrow \sigma^*(N–H)$ interactions are given in Figure 15b.

NICS. Studies have demonstrated that NICS is a useful indicator of aromaticity that usually correlates well with the other energetic, structural, and magnetic criteria for aromaticity.[19–21] Intermolecular interactions involving aromatic rings are important processes in both chemical and biological

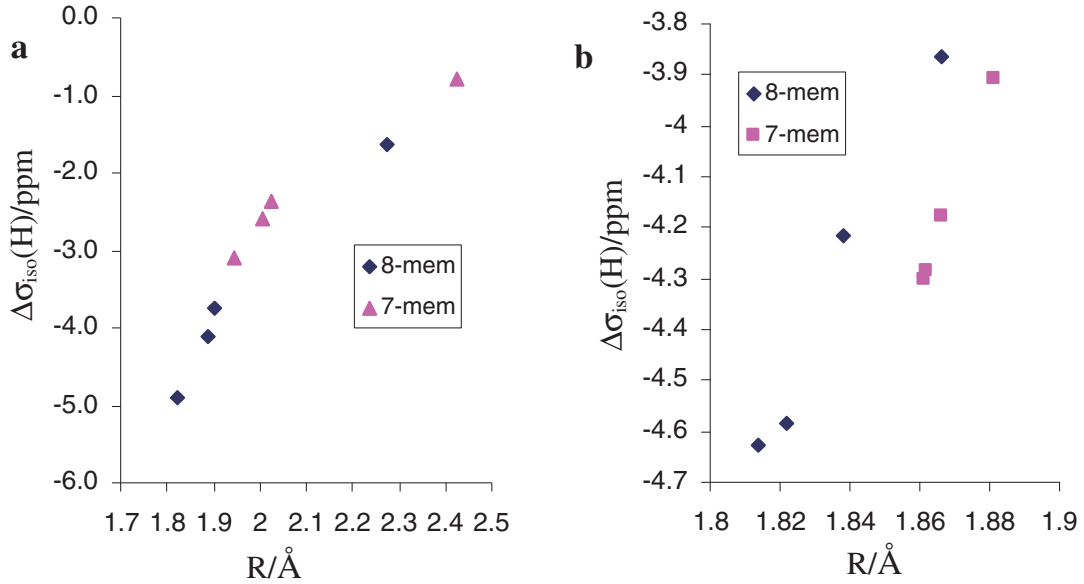

Figure 12. Correlation between change in isotropic chemical shift $\Delta\sigma_{iso}$(H)/ppm and (a) (H_U···Y) and (b) (H_{NA}···Y) H-bond distances (R).

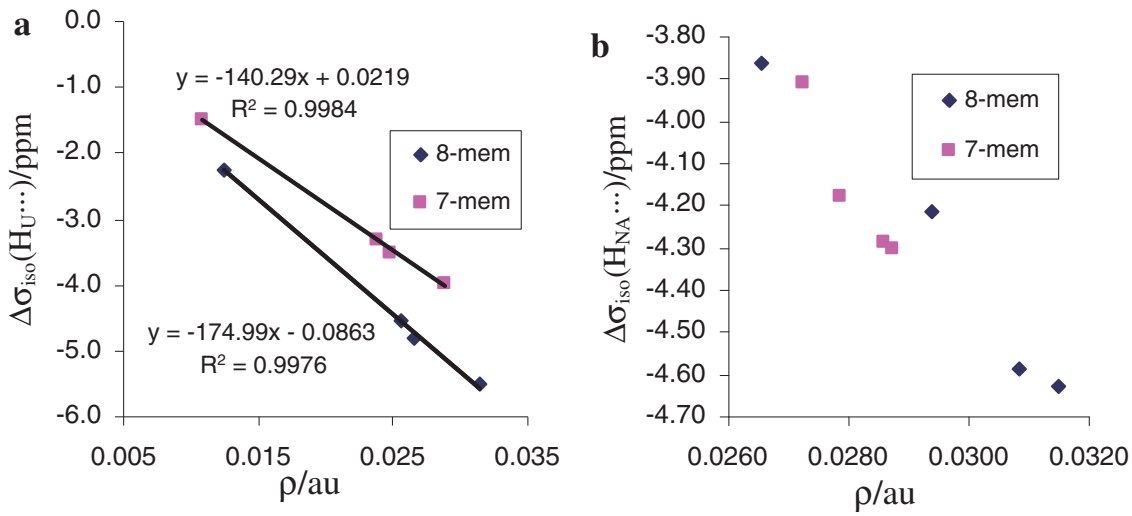

Figure 13. Relationship between $\Delta\sigma_{iso}(H_U\cdots)$ and electronic density, ρ, at (a) H_U···O(N) and (b) H_{NA}···O_U bond critical points.

recognition. Interaction **U** with **NA** can change the aromaticity of **U** ring. The values of NICS(0) and NICS(1) for **U** are −0.4788 and −1.1386 ppm, respectively (Table 6). The NICS(0) and NICS(1) values of a typical aromatic system, benzene, at B3LYP/6-311+G* level are −9.7 and −11.5 ppm, respectively.[32] Thus, in comparison with benzene, **U** is a nonaromatic compound. The absolute values of NICS increase upon complexation, with the exception of NICS(0) for **UN5**. NICS values at the geometric center of the ring, NICS(0), contain important spurious contributions from the in-plane tensor components that are not related to aromaticity. NICS(1) (1 Å above/below the plane of the ring) essentially reflects π effects and it is a better indicator of the ring current than the value at the center, because at 1 Å the effects of the local π-bonding contributions are diminished.[26,33] Increase in NICS(1) value to form the **UN1–8** complexes is 31.2, 31.7, 14.9, 18.6, 9.2, 13.9, 28.1, and 25.6 percent, respectively. As a result, aromaticity of **U** ring reasonably increases upon complex formation of **UN1**, **UN2**, **UN7**, and **UN8**.

Table 6. NICS Aromaticity Indices Calculated at B3LYP/6-311++G(2d,2p)//MP2/6-311++G(2d,2p) Level

	NICS(0)	NICS(1)	|ΔNICS(0)|	|ΔNICS(1)|
U	−0.4788	−1.1386	0	0
UN1	−0.7722	−1.4943	0.2934	0.3557
UN3	−0.5738	−1.3084	0.095	0.1698
UN5	−0.4363	−1.2431	−0.0425	0.1045
UN7	−0.815	−1.4585	0.3362	0.3199
UN2	−0.7473	−1.499	0.2685	0.3604
UN4	−0.5875	−1.3504	0.1087	0.2118
UN6	−0.4815	−1.2969	0.0027	0.1583
UN8	−0.7852	−1.4306	0.3064	0.292

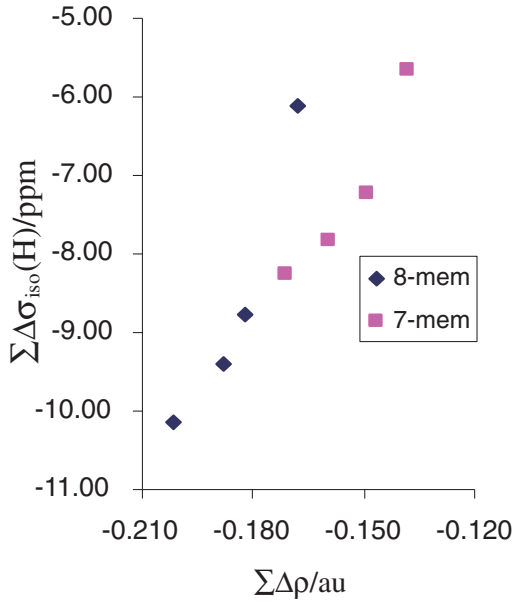

Figure 14. Correlation between the sum of change in isotropic chemical shift $\Delta\sigma_{iso}$(H)/ppm and the sum of change in electronic density ($\Delta\rho$)/au of the H atoms involved in H-bonding.

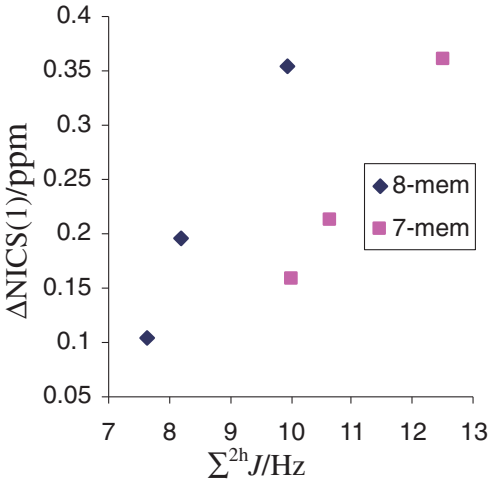

Figure 16. Correlation between ΔNICS(1) and the sum of $^{2h}J_{O\cdots N}$ and $^{2h}J_{N\cdots N(O)}$ SSCCs in eight- and seven-membered ring complexes.

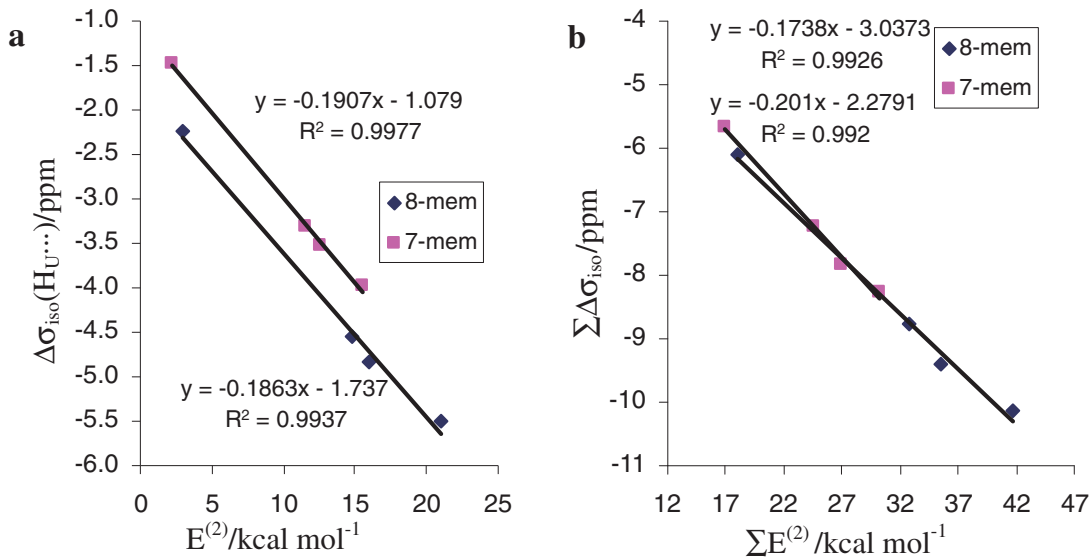

Figure 15. Correlation between (a) $\Delta\sigma_{iso}(H_U\cdots)$ and the corresponding charge-transfer energy $E^{(2)}$ for $LP(N(O))_{NA} \rightarrow \sigma^*(N(C)–H)$ interaction and (b) the sum of $\Delta\sigma_{iso}(H\cdots)$ and the sum of $E^{(2)}$ correspond to the $LP(N(O))_{NA} \rightarrow \sigma^*(N(C)–H)$ and $LP(O)_U \rightarrow \sigma^*(N–H)$ interactions.

There is a correlation between the ΔNICS(1) values and sum of $^{2h}J_{O\cdots N}$ and $^{2h}J_{N\cdots N(O)}$ SSCCs in **UN1**–**UN6** complexes. This correlation is presented in Figure 16. These curves show a linear connection between the ΔNICS(1) values and the sum of ^{2h}J in eight- and seven-membered ring complexes. As can be seen, increase in SSCCs in both types of complexes are connected with increase in the values of NICS(1).

Conclusion

In the present work, we have characterized hydrogen bonds formed from interaction between uracil (**U**) and parent nitrosamine (**NA**) for better understanding of the nature of hydrogen bonds. All eight complexes found on the potential surface have ring structures with two hydrogen bonds. We have computed binding energies, structural parameters, vibrational frequencies, electron density at HBCP, charge-transfer energies, SSCCs, isotropic chemical shifts, and NICS values. The correlation between spin–spin coupling constants ($^{1h}J_{H\cdots Y}$ and $^{2h}J_{X\cdots Y}$) and isotropic chemical shifts with the binding energy, H-bond distance, red shift of vibration frequency, charge-transfer energy, and electron density at H-bond critical point were investigated at the above-mentioned level of theory. Change in nucleus-independent chemical shift of **U** ring upon complex formation was also calculated.

Supporting Information

The spin–spin coupling constants calculated using cc-pVDZ basis set for **UN1** and **UN2**. This material is available free of charge on the web at http://www.csj.jp/journals/bcsj/.

References

1 G. A. Jeffrey, W. Saenger, *Hydrogen Bonding in Biological Structures*, Springer-Verlag, Berlin, **1991**.

2 G. A. Jeffrey, *An Introduction to Hydrogen Bonding*, Oxford University Press, New York, **1997**.

3 G. R. Desiraju, T. Steiner, *The Weak Hydrogen Bond: In Structural Chemistry and Biology*, Oxford University Press, Oxford, **1999**.

4 S. Scheiner, *Hydrogen Bonding: A Theoretical Perspective*, Oxford University Press, Oxford, **1997**.

5 K. Müller-Dethlefs, P. Hobza, *Chem. Rev.* **2000**, *100*, 143.

6 H. Cybulski, M. Pecul, J. Sadlej, *Chem. Phys.* **2006**, *326*, 431.

7 R. Ida, M. De Clerk, G. Wu, *J. Phys. Chem. A* **2006**, *110*, 1065.

8 a) N. Juranić, S. Macura, *J. Am. Chem. Soc.* **2001**, *123*, 4099. b) V. Sychrovský, J. Vacek, P. Hobza, L. Žídek, V. Sklenář, D. Cremer, *J. Phys. Chem. B* **2002**, *106*, 10242.

9 I. Alkorta, J. E. Del Bene, J. Elguero, O. Mó, M. Yáñez, *Theor. Chem. Acc.* **2009**, *124*, 187.

10 J. E. Del Bene, J. Elguero, *J. Phys. Chem. A* **2006**, *110*, 1128.

11 T. Helgaker, O. B. Lutnæs, M. Jaszuński, *J. Chem. Theory Comput.* **2007**, *3*, 86.

12 M. Pietrzak, M. F. Shibl, M. Bröring, O. Kühn, H.-H. Limbach, *J. Am. Chem. Soc.* **2007**, *129*, 296.

13 F. Cordier, S. Grzesiek, *J. Am. Chem. Soc.* **1999**, *121*, 1601.

14 A. J. Dingley, S. Grzesiek, *J. Am. Chem. Soc.* **1998**, *120*, 8293.

15 A. J. Dingley, F. Cordier, S. Grzesiek, *Concepts Magn. Reson.* **2001**, *13*, 103.

16 P. R. Blake, J. B. Park, M. W. W. Adams, M. F. Summers, *J. Am. Chem. Soc.* **1992**, *114*, 4931.

17 G. Cornilescu, B. E. Ramirez, M. K. Frank, G. M. Clore, A. M. Gronenborn, A. Bax, *J. Am. Chem. Soc.* **1999**, *121*, 6275.

18 I. G. Shenderovich, S. H. Smirnov, G. S. Denisov, V. A. Gindin, N. S. Golubev, A. Dunger, R. Reibke, S. Kirpekar, O. L. Malkina, H. H. Limbach, *Ber. Bunsen-Ges. Phys. Chem* **1998**, *102*, 422.

19 S. F. Boys, F. Bernardi, *Mol. Phys.* **1970**, *19*, 553.

20 T. Helgaker, M. Jaszuński, M. Pecul, *Prog. Nucl. Magn. Reson. Spectrosc.* **2008**, *53*, 249, and references cited therein.

21 N. F. Ramsey, *Phys. Rev.* **1950**, *78*, 699.

22 N. F. Ramsey, *Phys. Rev.* **1953**, *91*, 303.

23 T. Helgaker, M. Jaszuński, K. Ruud, *Chem. Rev.* **1999**, *99*, 293.

24 P. R. Schleyer, C. Maerker, A. Dransfeld, H. Jiao, N. J. R. E. Hommes, *J. Am. Chem. Soc.* **1996**, *118*, 6317.

25 P. R. Schleyer, H. Jiao, N. J. R. E. Hommes, V. G. Malkin, O. L. Malkina, *J. Am. Chem. Soc.* **1997**, *119*, 12669.

26 P. R. Schleyer, M. Manoharan, Z.-X. Wang, B. Kiran, H. Jiao, R. Puchta, N. J. R. E. Hommes, *Org. Lett.* **2001**, *3*, 2465.

27 R. Ditchfield, *Mol. Phys.* **1974**, *27*, 789.

28 K. Wolinski, J. F. Hinton, P. Pulay, *J. Am. Chem. Soc.* **1990**, *112*, 8251.

29 F. Biegler-König, J. Schönbohm, D. Bayles, *J. Comput. Chem.* **2001**, *22*, 545.

30 D. E. Glendening, A. E. Reed, J. E. Carpenter, F. Weinhold, *NBO, Version 3.1*.

31 M. J. Frisch, G. W. Trucks, H. B. Schlegel, G. E. Scuseria, M. A. Robb, J. R. Cheeseman, J. A. Montgomery, Jr., T. Vreven, K. N. Kudin, J. C. Burant, J. M. Millam, S. S. Iyengar, J. Tomasi, V. Barone, B. Mennucci, M. Cossi, G. Scalmani, N. Rega, G. A. Petersson, H. Nakatsuji, M. Hada, M. Ehara, K. Toyota, R. Fukuda, J. Hasegawa, M. Ishida, T. Nakajima, Y. Honda, O. Kitao, H. Nakai, M. Klene, X. Li, J. E. Knox, H. P. Hratchian, J. B. Cross, C. Adamo, J. Jaramillo, R. Gomperts, R. E. Stratmann, O. Yazyev, A. J. Austin, R. Cammi, C. Pomelli, J. W. Ochterski, P. Y. Ayala, K. Morokuma, G. A. Voth, P. Salvador, J. J. Dannenberg, V. G. Zakrzewski, S. Dapprich, A. D. Daniels, M. C. Strain, O. Farkas, D. K. Malick, A. D. Rabuck, K. Raghavachari, J. B. Foresman, J. V. Ortiz, Q. Cui, A. G. Baboul, S. Clifford, J. Cioslowski, B. B. Stefanov, G. Liu, A. Liashenko, P. Piskorz, I. Komaromi, R. L. Martin, D. J. Fox, T. Keith, M. A. Al-Laham, C. Y. Peng, A. Nanayakkara, M. Challacombe, P. M. W. Gill, B. Johnson, W. Chen, M. W. Wong, C. Gonzalez, J. A. Pople, *Gaussian 03 (Revision B.03)*, Gaussian Inc., Pittsburgh PA, **2003**.

32 H. Duan, Z. Gong, J. Cheng, W. Zhu, K. Chen, H. Jiang, *J. Phys. Chem. A* **2006**, *110*, 12236.

33 C. Corminboeuf, T. Heine, G. Seifert, P. R. Schleyer, J. Weber, *Phys. Chem. Chem. Phys.* **2004**, *6*, 273.